Title

4D CT lung ventilation images are affected by the 4D CT sorting method

Journal

Medical Physics, 40(10)

ISSN

0094-2405

Authors

Yamamoto, Tokihiro
Kabus, Sven
Lorenz, Cristian
et al.

Publication Date

2013-09-11

DOI

10.1118/1.4820538

Peer reviewed

4D CT lung ventilation images are affected by the 4D CT sorting method

Tokihiro Yamamoto
Department of Radiation Oncology, Stanford University School of Medicine, Stanford, California 94305-5847 and Department of Radiation Oncology, University of California Davis School of Medicine, Sacramento, California 95817

Sven Kabus and Cristian Lorenz
Department of Digital Imaging, Philips Research Europe, 22335 Hamburg, Germany

Eric Johnston, Peter G. Maxim, Maximilian Diehn, Neville Eclov, Cristian Barquero, and Billy W. Loo, Jr.[a)]
Department of Radiation Oncology, Stanford University School of Medicine, Stanford, California 94305-5847

Paul J. Keall[a)]
Sydney Medical School, University of Sydney, Blackburn Building D06, Sydney, New South Wales 2006, Australia

(Received 1 May 2013; revised 1 July 2013; accepted for publication 17 August 2013; published 11 September 2013)

Purpose: Four-dimensional (4D) computed tomography (CT) ventilation imaging is a novel promising technique for lung functional imaging. The current standard 4D CT technique using phase-based sorting frequently results in artifacts, which may deteriorate the accuracy of ventilation imaging. The purpose of this study was to quantify the variability of 4D CT ventilation imaging due to 4D CT sorting.
Methods: 4D CT image sets from nine lung cancer patients were each sorted by the phase-based method and anatomic similarity-based method, designed to reduce artifacts, with corresponding ventilation images created for each method. Artifacts in the resulting 4D CT images were quantified with the artifact score which was defined based on the difference between the normalized cross correlation for CT slices within a CT data segment and that for CT slices bordering the interface between adjacent CT data segments. The ventilation variation was quantified using voxel-based Spearman rank correlation coefficients for all lung voxels, and Dice similarity coefficients (DSC) for the spatial overlap of low-functional lung volumes. Furthermore, the correlations with matching single-photon emission CT (SPECT) ventilation images (assumed ground truth) were evaluated for three patients to investigate which sorting method provides higher physiologic accuracy.
Results: Anatomic similarity-based sorting reduced 4D CT artifacts compared to phase-based sorting (artifact score, 0.45 ± 0.14 vs 0.58 ± 0.24, $p = 0.10$ at peak-exhale; 0.63 ± 0.19 vs 0.71 ± 0.31, $p = 0.25$ at peak-inhale). The voxel-based correlation between the two ventilation images was 0.69 $\pm$ 0.26 on average, ranging from 0.03 to 0.85. The DSC was 0.71 ± 0.13 on average. Anatomic similarity-based sorting yielded significantly fewer lung voxels with paradoxical negative ventilation values than phase-based sorting ($5.0 \pm 2.6\%$ vs $9.7 \pm 8.4\%$, $p = 0.05$), and improved the correlation with SPECT ventilation regionally.
Conclusions: The variability of 4D CT ventilation imaging due to 4D CT sorting was moderate overall and substantial in some cases, suggesting that 4D CT artifacts are an important source of variations in 4D CT ventilation imaging. Reduction of 4D CT artifacts provided more physiologically convincing and accurate ventilation estimates. Further studies are needed to confirm this result.
 [http://dx.doi.org/10.1118/1.4820538]

Key words: lung, functional imaging, ventilation, four-dimensional (4D) CT, artifact

1. INTRODUCTION

Four-dimensional (4D) computed tomography (CT) ventilation imaging has emerged as a novel promising technique for lung functional imaging in the field of radiation oncology.[1] The 4D CT-derived ventilation can be considered "free" information for lung cancer radiotherapy patients, since 4D CT scans are currently in routine use for treatment planning purposes at many centers (estimated to be >50% based on Simpson *et al.*[2]) and ventilation computation involves only image processing and analysis. Moreover, 4D CT ventilation imaging has a higher resolution, lower cost, shorter scan time, and/or higher availability compared to competing techniques, e.g., single-photon emission CT (SPECT) and magnetic resonance (MR) imaging. If a 4D CT scan is not in routine use, it would require an extra dose of approximately 100 mGy (Ref. 3) and an exam time of 10–20 min. In the literature, there have been applications of 4D CT ventilation imaging to treatment planning for functional avoidance[4,5] and assessment of radiation-induced changes in pulmonary function.[6,7]

The animal subject studies have demonstrated reasonable correlations between 4D CT ventilation and xenon CT ventilation[8–10] and also high reproducibility[11] in healthy lungs. However, the human subject studies have reported low correlations between 4D CT ventilation and SPECT ventilation[12,13] and poor to moderate reproducibility[11,14] in diseased lungs with lung cancer, while Castillo *et al.*[15] have recently demonstrated strong correlations between functional defect regions distal to tumor-induced airway obstruction defined by 4D CT ventilation and SPECT perfusion. There are several major differences between the animal and human studies, including lung physiologic condition and 4D CT image acquisition. Animal studies used animals with healthy lungs, whereas human studies used patients with diseased lungs. The 4D CT ventilation cannot distinguish actual inflow of fresh gas (i.e., ventilation) from redistribution of alveolar or dead space gas (i.e., pendelluft[16]), which may be considerable in diseased lungs such as chronic obstructive pulmonary disease [COPD (Ref. 17)]. Most relevant to this study, the 4D CT images have been acquired during well-controlled tidal breathing with mechanical ventilation in the animal studies, whereas in the human studies most uncontrolled tidal breathing subject to variations throughout a scan. Although audio and/or visual biofeedback respiratory training has been employed by several investigators,[11,14] it has been based on patient's abdominal displacements, which do not necessarily represent internal lung motion,[18] and also there can still be residual variations. Respiratory variations result in artifacts in 4D CT images and also inconsistent lung volumes.[19] These factors may deteriorate the accuracy and/or reproducibility of 4D CT ventilation imaging in diseased human subjects, and might contribute to the conflicting results in the literature.

The purpose of this study was to quantify the variability of 4D CT ventilation imaging due to 4D CT sorting. The current standard 4D CT technique with phase-based sorting[20] results in artifacts at an alarmingly high frequency [90% (Ref. 19)], while there have been several improved sorting methods that reduce artifacts.[21–28] This study is the first to quantify the ventilation variation arising from different 4D CT sorting methods. In addition, we also investigated which provides higher physiologic accuracy by comparing with SPECT ventilation (assumed ground truth).

2. METHODS AND MATERIALS

2.A. Patients

We studied nine thoracic cancer patients (seven males and two females) with the average age of 67 years (range, 51–80 years). Patients were selected retrospectively without prior knowledge of 4D CT artifacts from those on two prospective clinical studies approved by Stanford University's Institutional Review Board. Both of these study protocols require 4D CT scans. All patients provided written informed consent.

2.B. 4D CT imaging and sorting: Phase-based and anatomic similarity-based

4D CT scans of the entire thorax were acquired on a Discovery ST multislice positron emission tomography (PET)/CT scanner (GE Healthcare, Waukesha, WI) in cine mode. Simultaneously, patient's abdominal displacements were measured using a real-time position management (RPM) system (Varian Medical Systems, Palo Alto, CA). Scan parameters were set as follows: 120 kVp, approximately 100 mAs per slice, 0.5 s gantry rotation, 0.45 s cine interval, and 2.5 mm slice thickness, as used clinically in our department. The CT data were continuously acquired for a cine duration that was approximately 1 s longer than the patient's estimated respiratory period. Since the axial coverage of the scanner was 2 cm (eight slices), the cine CT acquisition was performed at multiple couch positions to cover the entire thorax. The voxel dimension was 1 (approximate) × 1 (approximate) × 2.5 mm. Further details on the 4D CT image acquisition have been described elsewhere.[20]

The oversampled CT slices were then sorted into ten respiratory bins using two different methods: phase-based sorting and anatomic similarity-based sorting, yielding two 4D CT image sets per patient. Phase-based sorting is based on the nearest neighbor criterion where the CT data segment is selected such that the synchronized RPM phase is closest to the prescribed target phase at each couch position.[29] Phase-based sorting was performed using GE Advantage 4D software. Anatomic similarity-based sorting is designed to reduce 4D CT artifacts and is based on the correlation between CT slices bordering the interface between adjacent couch positions (i.e., anatomic similarity), synchronized RPM abdominal displacement, and direction of breathing (i.e., exhale or inhale). It selects candidate CT data segments about the prescribed target displacement based on the nearest neighbor criterion, followed by calculation of the correlation coefficients for all candidate CT slice pairs bordering couch interfaces. Finally, CT data segments are selected to maximize the correlation over the entire data set. Anatomic similarity-based sorting was performed using an inhouse developed program. Further details have been described by Johnston *et al.*[28] They observed significantly reduced artifacts with anatomic similarity-based sorting than phase-based sorting.

To quantitatively evaluate artifacts in the resulting 4D CT images, we employed the artifact score (AS) defined by

$$\mathrm{AS} = \frac{1}{N}\sum_{s=a}^{b}\left(\frac{\mathrm{NCC}(I[s,k-1],I[s,k]) + \mathrm{NCC}(I[s+1,1],I[s+1,2])}{2} - \mathrm{NCC}(I[s,k],I[s+1,1])\right)\cdot 100, \quad (1)$$

where NCC(I, I') is the normalized cross correlation (NCC) value between two CT slices (I and I'), $I[s, i]$ is the ith slice in the sth CT data segment, k is the number of slices per CT data segment ($k = 8$ for the scanner used here), a is the index of the CT data segment that contains the most superior slice of the lung, b is the index of the CT data segment that contains the most inferior slice of the lung, and N is the number of CT data segments that contain a lung. Note that 4D CT artifacts do not occur within a CT data segment. NCC($I[s, k-1]$, $I[s, k]$) and NCC($I[s+1, 1]$, $I[s+1, 2]$) reflect normal anatomic changes alone, while NCC($I[s, k]$, $I[s+1, 1]$) reflects possible artifact-caused decrease in anatomic similarity in addition to normal anatomic changes. Thus, the difference between these NCC values is positive in principle. The averaged difference is finally multiplied by a scale factor of 100 for ease of presentation. A NCC-based metric has been demonstrated to replicate the findings of human observers.[30] The artifact scores of the phase-sorted and anatomic similarity-sorted 4D CT images were compared using the two-tailed paired t-test.

2.C. 4D CT ventilation imaging

Two lung ventilation images were created from two 4D CT image sets generated by phase-based sorting and anatomic similarity-based sorting through (1) deformable image registration (DIR) for spatial mapping of the peak-exhale CT image to the peak-inhale image, and (2) quantification of regional air volume change. In this study, we used a volumetric elastic registration method that minimizes both a similarity function (sum of squared difference between the peak-inhale and deformed peak-exhale CT images) and a regularizing term (elastic regularizer) based on the Navier-Lamé equation.[31] Given that sliding motion of the lungs against the pleura can cause large registration errors, the DIR algorithm focused on only the lungs by assigning 0 HU to all the voxels with >0 HU. The registration accuracy was previously studied through quantifying the target registration error (distances between the anatomic landmarks including vessels and bronchial bifurcations) at the target phase propagated manually from the reference phase and those propagated by DIR. The target registration errors were found to be less than the voxel dimension on average.[31–33] The same algorithm parameters were employed in this study. To quantify regional air volume change, we employed the Jacobian-based ventilation metric.[9] The Jacobian determinant (J) of the displacement vector, u, is given by

$$J(x, y, z) = \begin{vmatrix} 1 + \frac{\partial u_x(x,y,z)}{\partial x} & \frac{\partial u_x(x,y,z)}{\partial y} & \frac{\partial u_x(x,y,z)}{\partial z} \\ \frac{\partial u_y(x,y,z)}{\partial x} & 1 + \frac{\partial u_y(x,y,z)}{\partial y} & \frac{\partial u_y(x,y,z)}{\partial z} \\ \frac{\partial u_z(x,y,z)}{\partial x} & \frac{\partial u_z(x,y,z)}{\partial y} & 1 + \frac{\partial u_z(x,y,z)}{\partial z} \end{vmatrix}, \quad (2)$$

which represents the differential expansion ($J > 1$), no volume change ($J = 1$), or contraction ($J < 1$) at point (x, y, z). Note that the scale of J is not linear, e.g., $J = 2$ and $J = 0$ represent different changes in volume. The volume of each exhale voxel deformed into the inhale phase ($\mathrm{Vol}_{\mathrm{in}}^{\mathrm{voxel}}$) can be estimated by

$$\mathrm{Vol}_{\mathrm{in}}^{\mathrm{voxel}}(x, y, z) = \mathrm{Vol}_{\mathrm{ex}}^{\mathrm{voxel}}(x, y, z) \cdot J(x, y, z), \quad (3)$$

where $\mathrm{Vol}_{\mathrm{ex}}^{\mathrm{voxel}}$ is the exhale voxel volume. In this study, the ventilation metric (V) was defined as exhale-to-inhale air volume change and can be expressed as

$$\begin{aligned} V(x, y, z) &= \mathrm{Vol}_{\mathrm{in}}^{\mathrm{voxel}}(x, y, z) - \mathrm{Vol}_{\mathrm{ex}}^{\mathrm{voxel}}(x, y, z) \\ &= \mathrm{Vol}_{\mathrm{ex}}^{\mathrm{voxel}} \cdot \{J(x, y, z) - 1\}. \end{aligned} \quad (4)$$

A positive ventilation value represents local expansion, while a negative value represents local contraction. Thus, ventilation images in the peak-exhale phase domain were created from the phase-sorted and anatomic similarity-sorted 4D CT images. Further details on 4D CT ventilation imaging have been described elsewhere.[34,35]

The ventilation values outside the segmented lung parenchyma volumes were zeroed before quantifying the variability. The lung volume was segmented by delineating lung voxels, of which the Hounsfield unit (HU) values were smaller than a threshold of −250 (Refs. 12, 15, and 36) within the lung outlines generated by the model-based segmentation of a Pinnacle^3 treatment planning system (Philips Radiation Oncology Systems, Fitchburg, WI). Manual trimming of the central airways and great vessels was also performed where necessary.

2.D. Quantification of the ventilation variability due to 4D CT sorting methods

The two ventilation images derived from the phase-sorted and anatomic similarity-sorted 4D CT images were compared to quantify the ventilation variability due to 4D CT sorting methods. The two ventilation images were rigidly aligned for quantitative analysis. The ventilation variation was evaluated by visual inspection and quantitative analysis using two metrics:

(1) Voxel-based Spearman rank correlation coefficients (ρ) for all voxels within the lung

(2) DSC (Ref. 37) for the spatial overlap of segmented low-functional lung volumes as defined by

$$\mathrm{DSC} = \frac{2 \cdot \mathrm{LFL}_{\mathrm{phase}} \cap \mathrm{LFL}_{\mathrm{anatomy}}}{\mathrm{LFL}_{\mathrm{phase}} + \mathrm{LFL}_{\mathrm{anatomy}}}, \quad (5)$$

where LFL is the low-functional lung volume.

Mismatched lung voxels between the two ventilation images were excluded and only the intersecting voxels were included in the analysis. Given that the two ventilation images were derived from two 4D CT images reflecting different patient's breathing levels, the ventilation values were globally normalized by the overall mean ventilation ($\overline{V}$) of each image as

$$V_n(x, y, z) = \frac{\mathrm{Vol}_{\mathrm{ex}}^{\mathrm{voxel}} \cdot \{J(x, y, z) - 1\}}{\overline{V}}. \quad (6)$$

The resulting normalized ventilation value is unitless. A positive value represents local expansion, while a negative value represents local contraction. The low-functional lung volume was defined as 33% lung volume with the lowest ventilation values. The cutoff values proposed by Zou *et al.*[38,39] were utilized to interpret the voxel-based correlation coefficients and DSCs in Sec. 4.

2.E. Comparison of 4D CT ventilation and SPECT ventilation

To investigate which of the two ventilation images provide higher physiologic accuracy, we qualitatively and quantitatively assessed the correlation with SPECT ventilation images (assumed ground truth). Out of nine patients, six patients (patients 1, 3–6, 8) received SPECT ventilation imaging with technetium-99m-labeled diethylenetriamine pentaacetate (^{99m}Tc-DTPA) aerosols as part of one of the two prospective clinical studies. SPECT ventilation scans including low-dose CT scans for attenuation correction were acquired on a GE Infinia Hawkeye SPECT/CT scanner. ^{99m}Tc-DTPA was aerosolized using an Insta/Vent system (Medi/Nuclear, Baldwin Park, CA) and was then administered to the patient in a supine posture through slow, moderately deep breathing. SPECT projections were acquired in a 64×64 matrix with a 8.8×8.8 mm^2 pixel size, 8.8 mm slice spacing, 60 projections over 360°, and 30 s per projection during tidal breathing. SPECT images were reconstructed using the 3D ordered-subsets expectation maximization (OSEM) algorithm with attenuation correction. Out of six patients, three patients were excluded from the analysis because of significant depositions of DTPA aerosols in central airways, which underrepresent ventilation in the peripheral lungs distal to those regions.[12,40] Thus, only patients 3, 6, and 8 were included in the analysis. Patients 3 and 6 received the SPECT and 4D CT scans before the start of radiotherapy treatment at an interval of 13 and 26 days, respectively. Patient 8 received both scans on the same day. To compare 4D CT ventilation and SPECT ventilation images, the low-dose CT image of SPECT was rigidly aligned with the peak-exhale 4D CT image using the image fusion feature of the Pinnacle^3 system. The resulting transformation matrix was then directly applied to the 4D CT ventilation image. For quantitative analysis, the DSCs for the spatial overlap between the segmented low-functional lung volumes (i.e., 33% lung volume with the lowest ventilation values) of 4D CT ventilation and those of SPECT ventilation were determined in a similar manner to quantification of the ventilation variability due to 4D CT sorting methods (see Sec. 2.D).

3. RESULTS

3.A. Comparison of 4D CT images generated by phase-based sorting and anatomic similarity-based sorting

Table I shows characteristics of the phase-sorted and anatomic similarity-sorted 4D CT images for the nine patients. The peak-exhale and peak-inhale lung volumes were determined using the segmentation method described above in Sec. 2.C. Overall, the two sorting methods resulted in comparable lung volumes and tidal volumes. However, there were considerable differences in several patients, e.g., 39% difference in patient 6 tidal volume, and 31% difference in patient 8 tidal volume. It was because lung volume segmentation was affected by artifacts, and because the phase-sorted and anatomic similarity-sorted 4D CT images were comprised of different CT data segments acquired at different breathing levels. Figure 1 shows a comparison of the 4D CT images sorted based on phase and anatomic similarity for patients 6 and 4. Patient 6 demonstrated the greatest decrease in the artifact score by anatomic similarity-based sorting compared to phase-based sorting. This patient had substantial respiratory variations right at the time of scanning diaphragms, resulting in severe artifacts as shown in the phase-sorted 4D CT images. Anatomic discontinuities around the diaphragms were reduced remarkably by anatomic similarity-based sorting at both peak-exhale and peak-inhale. In contrast, patient 4 demonstrated the smallest change in the artifact score as neither the phase-sorted nor anatomic similarity-sorted 4D CT images contained large artifacts. The two peak-inhale images represented exactly the same information, i.e., phase-based and anatomic similarity-based sorting selected the same CT data segments to create 3D CT volumes.

Figure 2 shows a summary of the artifact scores of the phase-sorted and anatomic similarity-sorted 4D CT images for nine patients. On average, anatomic similarity-based sorting decreased the artifact score from 0.58 ± 0.24 to 0.45 ± 0.14 ($p = 0.10$) at peak-exhale, and from 0.71 ± 0.31 to 0.63 ± 0.19 ($p = 0.25$) at peak-inhale as expected. Anatomic similarity-based sorting consistently yielded 4D CT images with smaller or comparable artifact scores for all patients except for patient 5 (peak-inhale).

3.B. Comparison of ventilation images derived from the phase-sorted and anatomic similarity-sorted 4D CT images

Figure 3 shows a comparison of the ventilation images derived from the phase-sorted and anatomic similarity-sorted

TABLE I. Characteristics of the phase-sorted and anatomic similarity-sorted 4D CT images for the nine patients.

Patient	4D CT sorting method	Peak-exhale lung volume (l)	Peak-inhale lung volume (l)	Tidal volume (l)
1	Phase-based	4.30	4.94	0.67
	Anatomic similarity-based	4.23	4.97	0.75
2	Phase-based	3.02	3.53	0.51
	Anatomic similarity-based	3.10	3.54	0.44
3	Phase-based	4.09	5.45	1.36
	Anatomic similarity-based	4.10	5.44	1.34
4	Phase-based	4.75	5.66	0.91
	Anatomic similarity-based	5.22	5.68	0.46
5	Phase-based	6.15	6.62	0.48
	Anatomic similarity-based	6.18	6.66	0.48
6	Phase-based	2.09	2.21	0.13
	Anatomic similarity-based	2.01	2.30	0.29
7	Phase-based	3.88	4.27	0.39
	Anatomic similarity-based	3.91	4.35	0.45
8	Phase-based	2.68	2.85	0.17
	Anatomic similarity-based	2.69	3.01	0.32
9	Phase-based	2.58	2.95	0.38
	Anatomic similarity-based	2.52	2.96	0.44
Average	Phase-based	3.72 ± 1.27	4.28 ± 1.49	0.55 ± 0.38
	Anatomic similarity-based	3.77 ± 1.35	4.32 ± 1.47	0.55 ± 0.32

4D CT images for patients 6 and 4. Patient 6, who showed the greatest decrease in the artifact score, demonstrated a voxel-based Spearman correlation of 0.62. There were marked disagreements around the lower lobes, in which significant 4D CT artifacts were observed in the phase-sorted image. Phase-based sorting provided a number of negative ventilation values in those regions, whereas anatomic similarity-based sorting yielded positive values. Considering that we quantified the exhale-to-inhale air volume change as defined by Eq. (4), positive ventilation values (i.e., regional expansion) are more physiologically convincing and negative ventilation values (i.e., regional contraction) are not supposed to appear in principle. However, we cannot rule out the possibility that some lung regions may contract during inhalation, especially in the diseased lungs. Patient 4, who showed the smallest change in the artifact score, demonstrated a voxel-based correlation of 0.85. Overall, very little disagreement was observed throughout the lungs, though anatomic similarity-based sorting provided some negative ventilation values around the right diaphragm, which would be attributed to a blurring (Fig. 1).

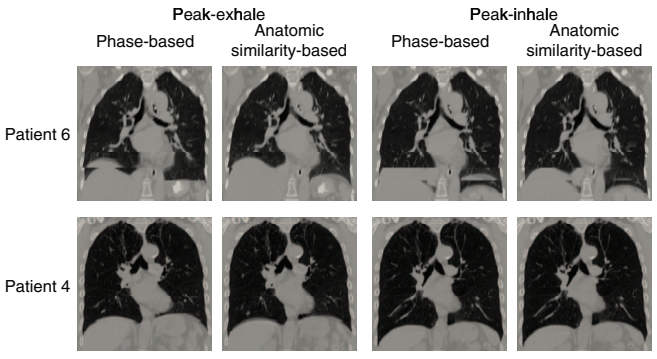

FIG. 1. 4D CT images (peak-exhale and peak-inhale) sorted based on phase and anatomic similarity for patients 6 and 4. Patient 6 showed the greatest decrease in the artifact score from 1.1 (phase-based) to 0.48 (anatomic similarity-based) at peak-exhale, and from 1.4 to 0.83 at peak-inhale. Patient 4 showed the smallest change in the artifact score from 0.42 to 0.43 at peak-exhale, and from 0.43 to 0.43 at peak-inhale.

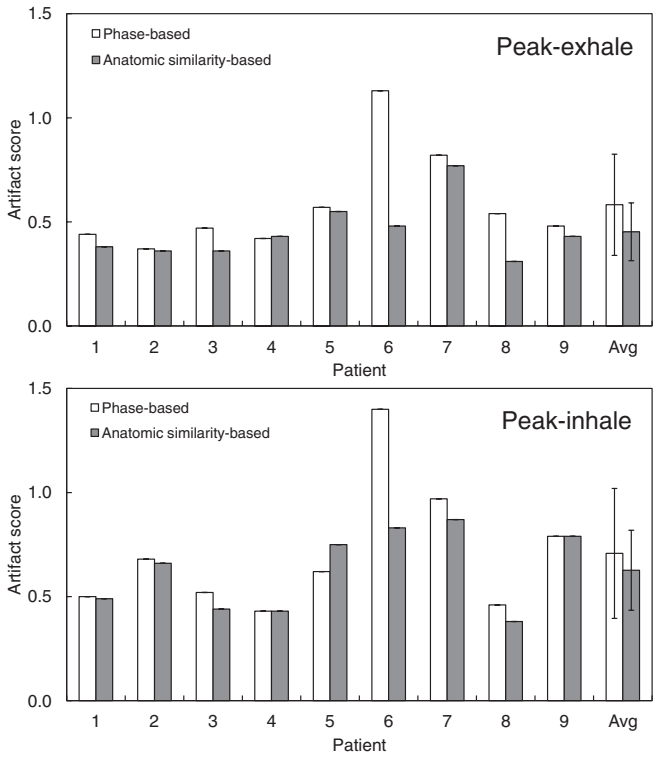

FIG. 2. Artifact scores of the 4D CT images (peak-exhale and peak-inhale) sorted based on phase and anatomic similarity for nine patients.

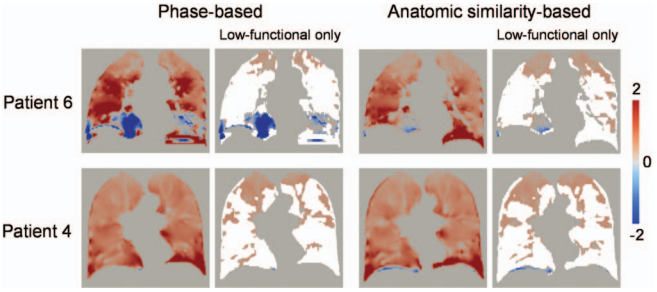

FIG. 3. Ventilation images derived from the phase-sorted and anatomic similarity-sorted 4D CT images for patients 6 and 4. The segmented low-functional lung volumes are also shown (nonlow functional lung volumes shaded white). Patients 6 and 4 demonstrated voxel-based Spearman correlations of 0.62 and 0.85, respectively. Note that ventilation is normalized by the overall mean value [see Eq. (6)]. A positive value represents local expansion, while a negative value represents local contraction. The coronal levels of the images are the same as those of Fig. 1.

Figure 4 demonstrates a summary of the DSCs and voxel-based correlation coefficients for nine patients. The DSC was found to be 0.71 ± 0.13 on average, ranging from 0.39 (patient 8) to 0.82 (patient 9). The voxel-based correlation was 0.69 ± 0.26 on average, ranging from 0.03 (patient 8) to 0.85 (patient 4). Compared with Fig. 2, lower correlations were not necessarily consistent with changes in the artifact score. For example, patient 2 showed a voxel-based correlation of 0.67, even though there was only a small change in the artifact score from 0.37 (phase-based) to 0.36 (anatomic similarity-based) at peak-exhale. Patient 8 demonstrated the lowest DSC and voxel-based correlation, which was due to a number of paradoxical negative ventilation values provided by phase-based sorting (29.3%) compared to anatomic similarity-based sorting (6.6%). It should be noted that patient 8 showed relatively small artifact scores for both phase-sorted and anatomic similarity-sorted 4D CT images (Fig. 2), since artifacts occurred in low contrast regions (i.e., lung parenchyma) and did not contribute much to the artifact score. Nevertheless, anatomic similarity-based sorting decreased the artifact score at both peak-exhale and peak-inhale.

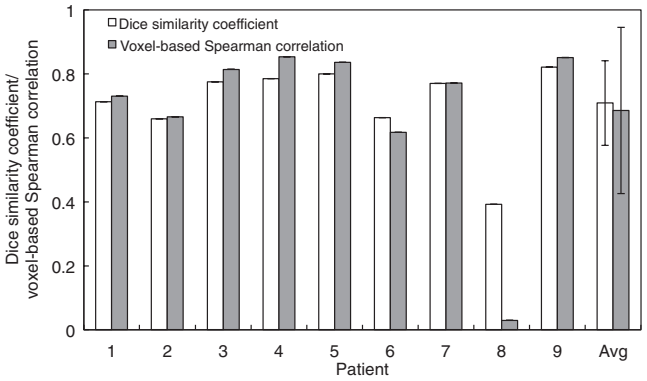

FIG. 4. Dice similarity coefficients (segmented low-functional lung regions) and voxel-based Spearman correlation coefficients (all voxels within the lung) between the ventilation images derived from the phase-sorted and anatomic similarity-sorted 4D CT images for nine patients.

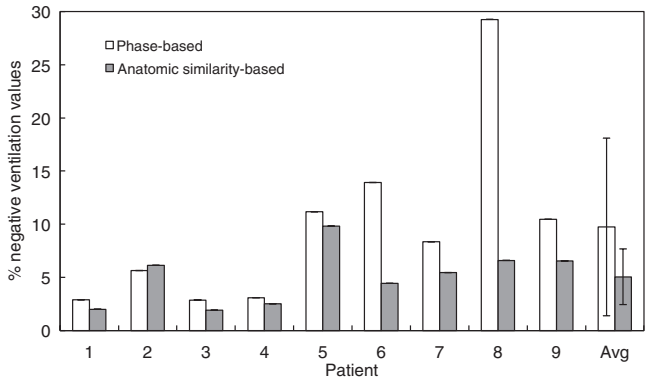

FIG. 5. The percentage of lung voxels with negative values in the ventilation images derived from the phase-sorted and anatomic similarity-sorted 4D CT images for nine patients.

Figure 5 shows a summary of the percentage of lung voxels with negative ventilation values provided by phase-based and anatomic similarity-based sorting for nine patients. On average, anatomic similarity-based sorting yielded a significantly fewer negative ventilation values than phase-based sorting (5.0 ± 2.6% vs 9.7 ± 8.4%, $p = 0.05$). Furthermore, we found a significant correlation between the artifact score of the 4D CT image and percentage of lung voxels with negative ventilation values ($R = 0.56$, $p = 0.02$) as shown in Fig. 6. These results indicate that reduction of 4D CT artifacts provides more physiologically convincing ventilation estimates.

Figure 7 shows the comparison of the two 4D CT ventilation images and SPECT ventilation image for three patients. Patients 6 and 8 demonstrated a marked change from paradoxical negative to positive ventilation in the lower and middle regions, respectively. These regions were found to have high ventilation as observed in the SPECT ventilation images, suggesting that reduction of 4D CT artifacts increases physiologic accuracy of ventilation estimates. However, a

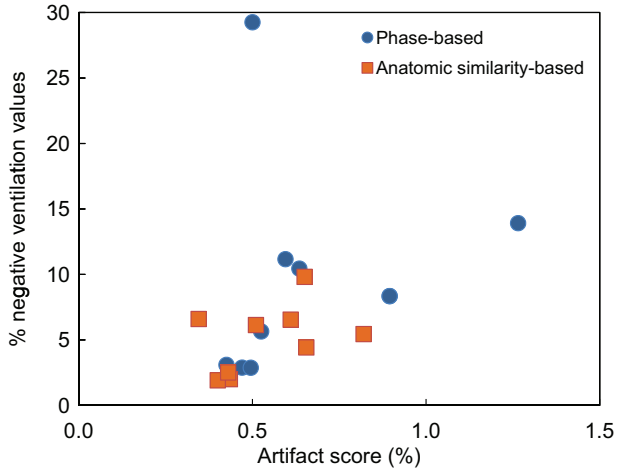

FIG. 6. Artifact scores of the 4D CT images (average of peak-exhale and peak-inhale) vs percentages of lung voxels with negative values in the ventilation images for nine patients, indicating a significant correlation ($R = 0.56$, $p = 0.02$).

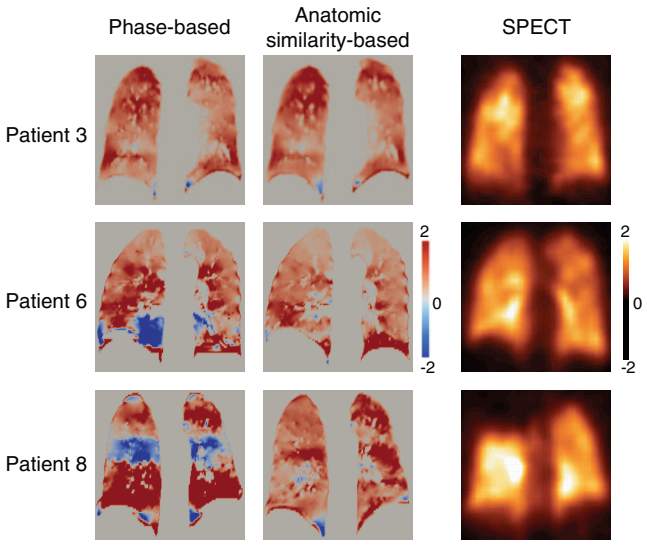

FIG. 7. 4D CT ventilation images (phase-based and anatomic similarity-based sorting) and SPECT ventilation image for patients 3, 6, and 8. Note that both 4D CT ventilation and SPECT ventilation are normalized by the overall mean value. A positive 4D CT ventilation value represents local expansion, while a negative value represents local contraction. A positive SPECT ventilation value represents local depositions of DTPA aerosols, while a negative value represents no depositions.

massive SPECT ventilation defect in the right upper lobe was not well estimated by 4D CT ventilation with either phase-based or anatomic similarity-based sorting. Patient 3 had a correlation of 0.81 between the two 4D CT ventilation images, both of which demonstrated reasonable correlations with SPECT ventilation. The DSCs for the spatial overlap between the segmented low-functional lung regions of 4D CT ventilation and those of SPECT ventilation increased slightly but consistently in all the three patients from 0.34, 0.40, and 0.24 (phase-based) to 0.39, 0.42, and 0.29 (anatomic similarity-based) in patients 3, 6, and 8, respectively.

4. DISCUSSION

This investigation is the first to quantify the variability of 4D CT ventilation imaging due to 4D CT sorting. We found that the ventilation variability was moderate overall and could be remarkable in some cases, depending on the particular nature or severity of 4D CT artifacts. Several investigators reported the effect of 4D CT artifacts on ventilation imaging. Castillo *et al.*[15] observed mismatch between 4D CT ventilation showing a cold-spot band arising from 4D CT artifacts and SPECT perfusion showing no functional defect in that region. More recently, Mathew *et al.*[41] also observed similar mismatch between 4D CT ventilation showing cold-spot and hyperpolarized ^{3}He MR ventilation showing no defect. Their results are consistent with our results, i.e., patients 6 and 8 demonstrated mismatch between 4D CT ventilation (phase-based) showing cold-spot and SPECT ventilation showing no defect (Fig. 7). Furthermore, we also demonstrated that reduction of 4D CT artifacts provided more physiologically convincing and accurate ventilation estimates with significantly reduced negative ventilation values and improved correlations with SPECT ventilation. Castillo *et al.*[15] and Mathew *et al.*[41] might have obtained higher correlations with SPECT perfusion and hyperpolarized ^{3}He MR ventilation, respectively, if 4D CT artifacts were mitigated as with our study. We have employed a commercially available sorting method (i.e., phase-based sorting), which is a standard in clinical practice, and a published method designed to reduce artifacts (i.e., anatomic similarity-based sorting). Investigation of other sorting methods such as displacement-based sorting[21,22,24] and internal anatomic feature-based sorting[27] could be a subject of future work.

4D CT ventilation imaging has been found to vary with DIR algorithms[35,42] and ventilation metrics to quantify regional air volume change.[10,35,42] This study has further suggested that 4D CT artifacts are another important source of variations in 4D CT ventilation. The animal subject studies have consistently demonstrated good physiologic accuracy and reproducibility of 4D CT ventilation imaging,[8–11] while the human subject studies have reported inconsistent results.[11–13,15] 4D CT image acquisition is one of the major differences between the animal and human studies. In the animal studies, the 4D CT images have been acquired during well-controlled tidal breathing with mechanical ventilation, yielding artifact-free 4D CT images. In contrast, in the human studies, the 4D CT images have been primarily acquired during uncontrolled tidal breathing that is subject to variations throughout a scan, yielding 4D CT images with potentially significant artifacts. It is therefore anticipated that 4D CT artifacts might have deteriorated the accuracy or reproducibility of ventilation imaging and contributed to inconsistent findings in the human studies. Several ventilation metrics based on different assumptions have been proposed in the literature.[1,9,10,14] All of those metrics are based on the basic assumption that the two image locations mapped by DIR represent two different respiratory phases (e.g., peak-exhale and peak-inhale). This assumption would not be valid in the presence of 4D CT artifacts, given that CT data segments with artifacts have a phase deviated from the target phase. Thus, 4D CT artifacts are considered to be an important source of variations in 4D CT ventilation, regardless of what metric is used to quantify regional air volume change. Nevertheless, it can be a subject of future work to investigate what metric would be more robust to 4D CT artifacts.

In addition to improved sorting[21–28] as studied here, there have been several other strategies to improve 4D CT in the literature, including postprocessing,[43–45] respiratory training,[46–48] respiration-synchronized acquisition,[49–51] and a wide-area detector multidetector CT (MDCT).[52] These approaches have been demonstrated to improve 4D CT image quality, however, each approach has different disadvantages as described below. Postprocessing approaches create a 3D CT volume at a predefined breathing level by DIR-based image interpolation, which requires a heavy computational burden and a well-validated DIR algorithm. Respiratory training (e.g., audiovisual biofeedback) to improve respiratory regularity requires patient compliance and may not work well especially for those with poor pulmonary function.

Respiration-synchronized acquisition approaches gate image acquisition based on predefined tolerances of the breathing level (e.g., phase and displacement) and real-time monitoring of the respiratory signal, which prolong the acquisition time and have not been implemented for actual scans. A new generation wide-area detector MDCT enables most of the thorax to be scanned at a single couch position, yielding high quality 4D CT images, however, it has very limited availability. Nevertheless, the physiologic accuracy and/or reproducibility of 4D CT ventilation imaging may be increased by these strategies.

In this study, the 4D CT ventilation images have been created using only peak-exhale and peak-inhale CT images yielding ventilation images in the peak-exhale phase domain, while the SPECT ventilation images have been acquired during tidal breathing over many respiratory cycles yielding blurred ventilation images. There have been no attempts to create blurred or averaged ventilation images with 4D CT in the literature to the best of our knowledge. Future work will utilize all the ten respiratory phases of 4D CT images to create burred or averaged ventilation images, which would, in principle, represent physiology during tidal breathing more accurately and may improve the correlation with SPECT ventilation.

5. CONCLUSIONS

We quantified the variability of 4D CT ventilation imaging due to 4D CT sorting for nine lung cancer patients. Variations in 4D CT ventilation were found to be moderate overall and substantial in some cases. Our results suggest that 4D CT artifacts are an important source of variations in 4D CT ventilation. Reduction of 4D CT artifacts provided more physiologically convincing and accurate ventilation estimates. Further studies are needed to confirm this result.

ACKNOWLEDGMENTS

This study was supported in part by National Lung Cancer Partnership Young Investigator Research Grant and NIH/NCI R01 93626. The authors are grateful to Michael L. Goris, M.D., Ph.D., Erik S. Mittra, M.D., Ph.D., and Lindee Burton of the Department of Radiology at Stanford for their support for SPECT image acquisition. The authors also thank Philips Radiation Oncology Systems for loaning Pinnacle[3] treatment planning systems.

[a]Authors to whom correspondence should be addressed. Electronic addresses: BWLoo@stanford.edu and Paul.Keall@sydney.edu.au

[1]T. Guerrero, K. Sanders, J. Noyola-Martinez, E. Castillo, Y. Zhang, R. Tapia, R. Guerra, Y. Borghero, and R. Komaki, "Quantification of regional ventilation from treatment planning CT," Int. J. Radiat. Oncol., Biol., Phys. **62**, 630–634 (2005).

[2]D. R. Simpson, J. D. Lawson, S. K. Nath, B. S. Rose, A. J. Mundt, and L. K. Mell, "Utilization of advanced imaging technologies for target delineation in radiation oncology," J. Am. Coll. Radiol. **6**, 876–883 (2009).

[3]M. J. Murphy, J. Balter, S. Balter, J. A. BenComo, Jr., I. J. Das, S. B. Jiang, C. M. Ma, G. H. Olivera, R. F. Rodebaugh, K. J. Ruchala, H. Shirato, and F. F. Yin, "The management of imaging dose during image-guided radiotherapy: Report of the AAPM Task Group 75," Med. Phys. **34**, 4041–4063 (2007).

[4]B. P. Yaremko, T. M. Guerrero, J. Noyola-Martinez, R. Guerra, D. G. Lege, L. T. Nguyen, P. A. Balter, J. D. Cox, and R. Komaki, "Reduction of normal lung irradiation in locally advanced non-small-cell lung cancer patients, using ventilation images for functional avoidance," Int. J. Radiat. Oncol., Biol., Phys. **68**, 562–571 (2007).

[5]T. Yamamoto, S. Kabus, J. von Berg, C. Lorenz, and P. J. Keall, "Impact of four-dimensional computed tomography pulmonary ventilation imaging-based functional avoidance for lung cancer radiotherapy," Int. J. Radiat. Oncol., Biol., Phys. **79**, 279–288 (2011).

[6]K. Ding, J. E. Bayouth, J. M. Buatti, G. E. Christensen, and J. M. Reinhardt, "4DCT-based measurement of changes in pulmonary function following a course of radiation therapy," Med. Phys. **37**, 1261–1272 (2010).

[7]Y. Y. Vinogradskiy, R. Castillo, E. Castillo, A. Chandler, M. K. Martel, and T. Guerrero, "Use of weekly 4DCT-based ventilation maps to quantify changes in lung function for patients undergoing radiation therapy," Med. Phys. **39**, 289–298 (2012).

[8]M. K. Fuld, R. B. Easley, O. I. Saba, D. Chon, J. M. Reinhardt, E. A. Hoffman, and B. A. Simon, "CT-measured regional specific volume change reflects regional ventilation in supine sheep," J. Appl. Physiol. **104**, 1177–1184 (2008).

[9]J. M. Reinhardt, K. Ding, K. Cao, G. E. Christensen, E. A. Hoffman, and S. V. Bodas, "Registration-based estimates of local lung tissue expansion compared to xenon CT measures of specific ventilation," Med. Image Anal. **12**, 752–763 (2008).

[10]K. Ding, K. Cao, M. K. Fuld, K. Du, G. E. Christensen, E. A. Hoffman, and J. M. Reinhardt, "Comparison of image registration based measures of regional lung ventilation from dynamic spiral CT with Xe-CT," Med. Phys. **39**, 5084–5098 (2012).

[11]K. Du, J. E. Bayouth, K. Cao, G. E. Christensen, K. Ding, and J. M. Reinhardt, "Reproducibility of registration-based measures of lung tissue expansion," Med. Phys. **39**, 1595–1608 (2012).

[12]R. Castillo, E. Castillo, J. Martinez, and T. Guerrero, "Ventilation from four-dimensional computed tomography: Density versus Jacobian methods," Phys. Med. Biol. **55**, 4661–4685 (2010).

[13]T. Yamamoto, S. Kabus, J. von Berg, C. Lorenz, M. L. Goris, B. W. Loo, Jr., and P. J. Keall, "Evaluation of four-dimensional (4D) computed tomography (CT) pulmonary ventilation imaging by comparison with single photon emission computed tomography (SPECT) scans for a lung cancer patient," in *Proceedings of the Third International Workshop on Pulmonary Image Analysis, MICCAI, Beijing, China, 2010* (2010), pp. 117–128.

[14]T. Yamamoto, S. Kabus, J. von Berg, C. Lorenz, M. P. Chung, J. C. Hong, B. W. Loo, Jr., and P. J. Keall, "Reproducibility of four-dimensional computed tomography-based lung ventilation imaging," Acad. Radiol. **19**, 1554–1565 (2012).

[15]R. Castillo, E. Castillo, M. McCurdy, D. R. Gomez, A. M. Block, D. Bergsma, S. Joy, and T. Guerrero, "Spatial correspondence of 4D CT ventilation and SPECT pulmonary perfusion defects in patients with malignant airway stenosis," Phys. Med. Biol. **57**, 1855–1871 (2012).

[16]B. A. Simon, D. W. Kaczka, A. A. Bankier, and G. Parraga, "What can computed tomography and magnetic resonance imaging tell us about ventilation?," J. Appl. Physiol. **113**, 647–657 (2012).

[17]A. Vyshedskiy and R. Murphy, "Pendelluft in chronic obstructive lung disease measured with lung sounds," Pulm. Med. **2012**, 139395 (2012).

[18]T. Iwasawa, Y. Yoshiike, K. Saito, S. Kagei, T. Gotoh, and S. Matsubara, "Paradoxical motion of the hemidiaphragm in patients with emphysema," J. Thorac. Imaging **15**, 191–195 (2000).

[19]T. Yamamoto, U. Langner, B. W. Loo, Jr., J. Shen, and P. J. Keall, "Retrospective analysis of artifacts in four-dimensional CT images of 50 abdominal and thoracic radiotherapy patients," Int. J. Radiat. Oncol., Biol., Phys. **72**, 1250–1258 (2008).

[20]E. Rietzel, T. Pan, and G. T. Chen, "Four-dimensional computed tomography: Image formation and clinical protocol," Med. Phys. **32**, 874–889 (2005).

[21]M. J. Fitzpatrick, G. Starkschall, J. A. Antolak, J. Fu, H. Shukla, P. J. Keall, P. Klahr, and R. Mohan, "Displacement-based binning of time-dependent computed tomography image data sets," Med. Phys. **33**, 235–246 (2006).

[22]W. Lu, P. J. Parikh, J. P. Hubenschmidt, J. D. Bradley, and D. A. Low, "A comparison between amplitude sorting and phase-angle sorting using external respiratory measurement for 4D CT," Med. Phys. **33**, 2964–2974 (2006).

[23]E. Rietzel and G. T. Chen, "Improving retrospective sorting of 4D computed tomography data," Med. Phys. **33**, 377–379 (2006).
[24]A. F. Abdelnour, S. A. Nehmeh, T. Pan, J. L. Humm, P. Vernon, H. Schoder, K. E. Rosenzweig, G. S. Mageras, E. Yorke, S. M. Larson, and Y. E. Erdi, "Phase and amplitude binning for 4D-CT imaging," Phys. Med. Biol. **52**, 3515–3529 (2007).
[25]Y. D. Mutaf, J. A. Antolak, and D. H. Brinkmann, "The impact of temporal inaccuracies on 4DCT image quality," Med. Phys. **34**, 1615–1622 (2007).
[26]T. Pan, X. Sun, and D. Luo, "Improvement of the cine-CT based 4D-CT imaging," Med. Phys. **34**, 4499–4503 (2007).
[27]R. Li, J. H. Lewis, L. I. Cervino, and S. B. Jiang, "4D CT sorting based on patient internal anatomy," Phys. Med. Biol. **54**, 4821–4833 (2009).
[28]E. Johnston, M. Diehn, J. D. Murphy, B. W. Loo, Jr., and P. G. Maxim, "Reducing 4D CT artifacts using optimized sorting based on anatomic similarity," Med. Phys. **38**, 2424–2429 (2011).
[29]T. Pan, T. Y. Lee, E. Rietzel, and G. T. Chen, "4D-CT imaging of a volume influenced by respiratory motion on multi-slice CT," Med. Phys. **31**, 333–340 (2004).
[30]G. Cui, B. Jew, J. C. Hong, E. W. Johnston, B. W. Loo, Jr., and P. G. Maxim, "An automated method for comparing motion artifacts in cine four-dimensional computed tomography images," J. Appl. Clin. Med. Phys. **13**, 170–180 (2012).
[31]S. Kabus and C. Lorenz, "Fast elastic image registration," in *Proceedings of the Medical Image Analysis For The Clinic: A Grand Challenge, MICCAI, Beijing, China, 2010* (2010), pp. 81–89.
[32]S. Kabus, J. von Berg, T. Yamamoto, R. Opfer, and P. J. Keall, "Lung ventilation estimation based on 4D-CT imaging," in *Proceedings of the First International Workshop on Pulmonary Image Analysis, MICCAI, New York, NY, 2008* (2008), pp. 73–81.
[33]S. Kabus, T. Klinder, K. Murphy, B. van Ginneken, C. Lorenz, and J. P. W. Pluim, "Evaluation of 4D-CT lung registration," in *Proceedings of the MICCAI*, edited by G. Z. Yang, D. J. Hawkes, D. Rueckert, J. A. Noble, and C. J. Taylor (Springer-Verlag, Berlin Heidelberg, London, UK, 2009), pp. 747–754.
[34]T. Yamamoto, S. Kabus, T. Klinder, C. Lorenz, J. von Berg, T. Blaffert, B. W. Loo, and P. J. Keall, "Investigation of four-dimensional computed tomography-based pulmonary ventilation imaging in patients with emphysematous lung regions," Phys. Med. Biol. **56**, 2279–2298 (2011).
[35]T. Yamamoto, S. Kabus, T. Klinder, J. von Berg, C. Lorenz, B. W. Loo, Jr., and P. J. Keall, "Four-dimensional computed tomography pulmonary ventilation images vary with deformable image registration algorithms and metrics," Med. Phys. **38**, 1348–1358 (2011).
[36]T. Guerrero, K. Sanders, E. Castillo, Y. Zhang, L. Bidaut, T. Pan, and R. Komaki, "Dynamic ventilation imaging from four-dimensional computed tomography," Phys. Med. Biol. **51**, 777–791 (2006).
[37]L. R. Dice, "Measures of the amount of ecologic association between species," Ecology **26**, 297–302 (1945).
[38]K. H. Zou, K. Tuncali, and S. G. Silverman, "Correlation and simple linear regression," Radiology **227**, 617–622 (2003).
[39]K. H. Zou, S. K. Warfield, A. Bharatha, C. M. Tempany, M. R. Kaus, S. J. Haker, W. M. Wells, III, F. A. Jolesz, and R. Kikinis, "Statistical validation of image segmentation quality based on a spatial overlap index," Acad. Radiol. **11**, 178–189 (2004).
[40]J. Petersson, A. Sanchez-Crespo, S. A. Larsson, and M. Mure, "Physiological imaging of the lung: Single-photon-emission computed tomography (SPECT)," J. Appl. Physiol. **102**, 468–476 (2007).
[41]L. Mathew, A. Wheatley, R. Castillo, E. Castillo, G. Rodrigues, T. Guerrero, and G. Parraga, "Hyperpolarized (3)He magnetic resonance imaging: comparison with four-dimensional x-ray computed tomography imaging in lung cancer," Acad. Radiol. **19**, 1546–1553 (2012).
[42]K. Latifi, G. Zhang, W. van Elmpt, S. Hoffe, T. Dilling, M. Stawicki, A. Dekker, and K. M. Forster, "Evaluation of the differences between locoregional lung ventilation estimation methods using a single deformable image registration algorithm," Med. Phys. **38**, 3387 (2011) (Abstract).
[43]E. Schreibmann, G. T. Chen, and L. Xing, "Image interpolation in 4D CT using a B-spline deformable registration model," Int. J. Radiat. Oncol., Biol., Phys. **64**, 1537–1550 (2006).
[44]S. Xu, R. H. Taylor, G. Fichtinger, and K. Cleary, "Lung deformation estimation and four-dimensional CT lung reconstruction," Acad. Radiol. **13**, 1082–1092 (2006).
[45]J. Ehrhardt, R. Werner, D. Saring, T. Frenzel, W. Lu, D. Low, and H. Handels, "An optical flow based method for improved reconstruction of 4D CT data sets acquired during free breathing," Med. Phys. **34**, 711–721 (2007).
[46]V. R. Kini, S. S. Vedam, P. J. Keall, S. Patil, C. Chen, and R. Mohan, "Patient training in respiratory-gated radiotherapy," Med. Dosim. **28**, 7–11 (2003).
[47]R. George, T. D. Chung, S. S. Vedam, V. Ramakrishnan, R. Mohan, E. Weiss, and P. J. Keall, "Audio-visual biofeedback for respiratory-gated radiotherapy: Impact of audio instruction and audio-visual biofeedback on respiratory-gated radiotherapy," Int. J. Radiat. Oncol., Biol., Phys. **65**, 924–933 (2006).
[48]R. B. Venkat, A. Sawant, Y. Suh, R. George, and P. J. Keall, "Development and preliminary evaluation of a prototype audiovisual biofeedback device incorporating a patient-specific guiding waveform," Phys. Med. Biol. **53**, N197–N208 (2008).
[49]P. J. Keall, S. S. Vedam, R. George, and J. F. Williamson, "Respiratory regularity gated 4D CT acquisition: Concepts and proof of principle," Australas Phys. Eng. Sci. Med. **30**, 211–220 (2007).
[50]U. W. Langner and P. J. Keall, "Prospective displacement and velocity-based cine 4D CT," Med. Phys. **35**, 4501–4512 (2008).
[51]U. W. Langner and P. J. Keall, "Quantification of artifact reduction with real-time cine four-dimensional computed tomography acquisition methods," Int. J. Radiat. Oncol., Biol., Phys. **76**, 1242–1250 (2010).
[52]C. Coolens, S. Breen, T. G. Purdie, A. Owrangi, J. Publicover, S. Bartolac, and D. A. Jaffray, "Implementation and characterization of a 320-slice volumetric CT scanner for simulation in radiation oncology," Med. Phys. **36**, 5120–5127 (2009).